Spectral Super-resolution for RGB Images Using Class-based BP Neural Networks

Xiaolin Han[1], Jing Yu[2], Jing-Hao Xue[3] and Weidong Sun[1]

1. State Key Laboratory of Intelligent Technology and Systems,
Beijing National Research Center for Information Science and Technology;
Department of Electronic Engineering, Tsinghua Univ., Beijing 100084, China
2. College of Computer Science and Technology, Beijing Univ. of Technology, Beijing100124, China
3. Department of Statistical Science, University College London, London, WC1E 6BT, U.K.

***Abstract*—Hyperspectral images are of high spectral resolution and have been widely used in many applications, but the imaging process to achieve high spectral resolution is at the expense of spatial resolution. This paper aims to construct a high-spatial-resolution hyperspectral (HHS) image from a high-spatial-resolution RGB image, by proposing a novel class-based spectral super-resolution method. With the help of a set of RGB and HHS image-pairs, our proposed method learns nonlinear spectral mappings between RGB and HHS image-pairs using class-based back propagation neural networks (BPNNs). In the training stage, unsupervised clustering is used to divide an RGB image into several classes according to spectral correlation, and the spectrum-pairs from the classified RGB images and the corresponding HHS images are used to train the BPNNs, to establish the nonlinear spectral mapping for each class. In the spectral super-resolution stage, a supervised classification is used to classify the given RGB image into the classes determined during the training stage, and the final HHS image is reconstructed from the classified given RGB image using the trained BPNNs. Comparisons on three standard datasets, ICVL, CAVE and NUS, demonstrate that, our proposed method achieves a better spectral super-resolution quality than related state-of-the-art methods.**

***Keywords*—spectral super-resolution, BP neural network, spectral classification, spectral mapping**

I. Introduction

Hyperspectral (HS) images with tens or hundreds of spectral bands can provide abundant spectral information, and have been widely used in environment monitoring [1][2], image classification [3][4], target detection [5][6] and so on. However, the imaging process to achieve high spectral resolution is at the expense of spatial resolution [7]. Compared with HS images, RGB images usually have much higher spatial resolution, but only have three spectral bands, and this greatly limits its effectiveness in the above-mentioned applications. Fortunately, the spectral information lost in RGB image may be recovered using the relationship between RGB and high-spatial-resolution hyperspectral (HHS) image-pairs provided by some generalized image databases. In other words, spectral super-resolution of RGB image is an alternative way to obtain the HHS image, if we can establish the spectral mapping from RGB to the hyperspectral spectral bands, using a large number of RGB and HHS image-pair samples.

Spectral super-resolution methods can be mainly divided into two groups: dictionary learning based and neural network based methods. Among the dictionary learning based methods, Arad *et al.* [8] have proposed a sparse representation method to obtain hyperspectral images from RGB images. Specifically, a spectral dictionary for hyperspectral and the corresponding RGB image-pairs is learned, using the hyperspectral image priors provided by the K-singular value decomposition (K-SVD) algorithm [9]. The sparse coefficients are estimated by the greedy orthogonal matching pursuit (OMP) algorithm [10] for the spectral dictionary learned above. To further improve the quality of reconstructed HHS image, Aeschbacher *et al.* [11] have re-implemented the above method [8] for better accuracy and runtime, and also proposed a shallow learned spectral reconstruction method based on the A+ method proposed for fast spatial super-resolution [12]. The comparable performance of [11] indicates its feasibility in the spectral super-resolution.

In order to further accurately establish the spectral mapping under a large number of RGB and HHS image-pair samples, neural network based methods have been developed very recently. Nguyen *et al.* [13] have proposed a radial basis function network based method to reconstruct a hyperspectral response from a single RGB image, with known spectral response function. It is a nonlinear mapping with a white-balancing process to reduce the effect of different illumination conditions. Galliani *et al.* [14] have proposed a deep convolutional neural network (CNN) method to learn an end-to-end mapping from RGB images to hyperspectral images. It has 56 layers, and can bring a better performance than that of the dictionary learning based methods. Inspired by the above methods, Can *et al.* [15] have proposed a rather shallow CNN method with residual blocks to learn the spectral mapping from RGB to HHS images. In addition, in order to increasing the number of image-pair samples for a better learning result, data augmentation [16] is also utilized, such as image rotating, flipping and downscaling. The common thread of the above CNN based methods is to establish the spectral mapping using image patches, such as a patch size of 36×36 used in [15] and a patch size of 64×64 used in [14], which means that the index space for spectral mapping is the texture provided by the

This work was supported in part by the National Natural Science Foundation of China (61501008), and Beijing Natural Science Foundation (4172002).

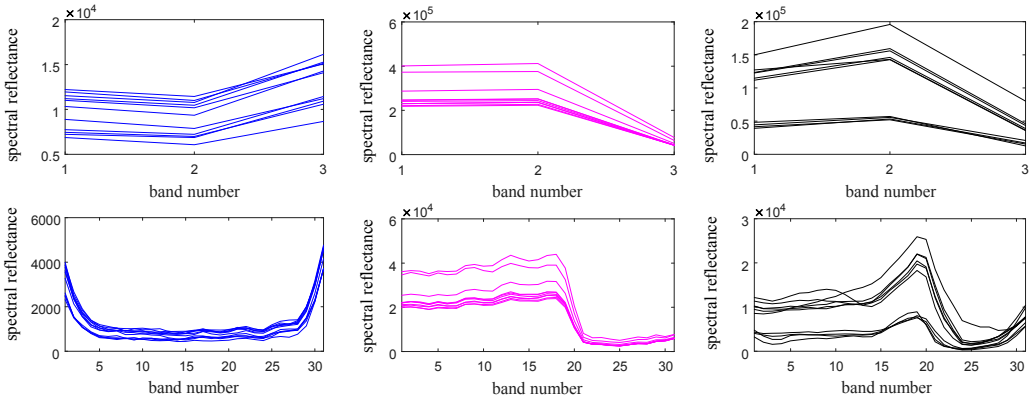

(a) class 1 (b) class 2 (c) class 3

Fig. 1 Spectral mappings of different classes using typical spectrum-pairs from RGB image (upper row) and the corresponding HHS image (lower row) in the CAVE dataset.

image patches, and the possible combination of such a large size image patches may leading to a huge requirements for the number of image-pair samples. That is one of the main reasons why data augmentation technique is also utilized in [16].

Considering it is more direct and efficient to use spectral domain as the index space, and the intrinsic characteristics that spectrum-pairs are more similar within each class of material than between classes and so do the corresponding spectral mapping. Hence in this paper, a novel spectral super-resolution method in the spectral domain is proposed to construct the HHS image from an RGB image, using class-based back propagation neural networks (BPNNs) [17]. In the training stage, unsupervised clustering is used to divide an RGB image into several classes according to spectral correlation, and the nonlinear spectral mappings for different classes are established using the spectrum-pairs from the classified RGB images and the corresponding HHS images by different BPNNs, respectively. In the spectral super-resolution stage, a supervised classification is used for the given RGB image to classify it into the classes determined during the training stage, and the final HHS image is reconstructed from the classified given RGB image using the trained BPNNs directly.

The main contributions of this paper are listed as follows.

1) To the best of our knowledge, this new framework for spectral super-resolution in the spectral domain based on the BPNNs is firstly given here.
2) A class-based BPNN learning method is proposed, to guarantee the similarity of spectral mappings from RGB to HHS images in each class.
3) An associative spectral classification is proposed, to ensure that the classes in the training and spectral super-resolution stages are consistent.

The rest of this paper is organized as follows. The proposed spectral super-resolution method is presented in Section II. Section III provides experimental results and discussions on different methods and datasets, followed by the conclusions in Section IV.

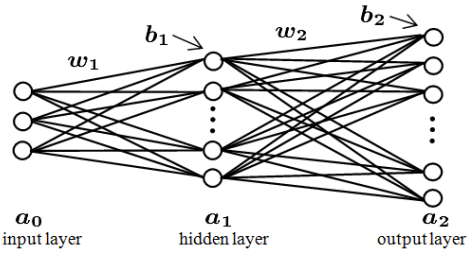

Fig.2 A three-layer BP neural network used in our proposed method.

II. Proposed Method

An RGB image $\mathbf{Y} \in \mathbb{R}^{3\times N}$ with three spectral bands can be seen as a spectral degradation of an HHS image $\mathbf{X} \in \mathbb{R}^{\lambda_\mathbf{X}\times N}$ by the spectral response function $\mathbf{L} \in \mathbb{R}^{3\times\lambda_\mathbf{X}}$:

$$\mathbf{Y} = \mathbf{L}\mathbf{X} + \mathbf{N}_\mathbf{Y} \tag{1}$$

where N represents the number of pixels per band, $\lambda_\mathbf{X}$ ($\lambda_\mathbf{X} \gg 3$) represents the number of spectral bands in $\mathbf{X}$, and $\mathbf{N}_\mathbf{Y}$ denotes the zero-mean Gaussian noise in the degradation model which is a popular assumption in the imaging process modeling [20][21].

According to the intrinsic characteristics that the similar spectrum-pairs in a single class are more similar than that in the total spectral domain and similar spectrum-pairs should have similar spectral mappings, the RGB image $\mathbf{Y}$ is divided into K classes. Besides, Fig.1 shows the spectral mappings of different classes using typical spectrum-pairs on the CAVE dataset [24], which will describe in more detail in Section III. As can be seen in Fig.1, the spectral mappings are much similar in each class, while they are much different among different classes. In this case, the spectral mapping of class i ($i = 1, ..., K$) from RGB to HHS can be described as

$$\mathbf{Y}^{c^{(i)}} = \mathbf{L}\mathbf{X}^{c^{(i)}} + \mathbf{N}_\mathbf{Y}^{c^{(i)}} \tag{2}$$

where $\mathbf{Y}^{c^{(i)}}$ and $\mathbf{X}^{c^{(i)}}$ denote the spectrums in class i of RGB image $\mathbf{Y}$ and HHS image $\mathbf{X}$, respectively. According to

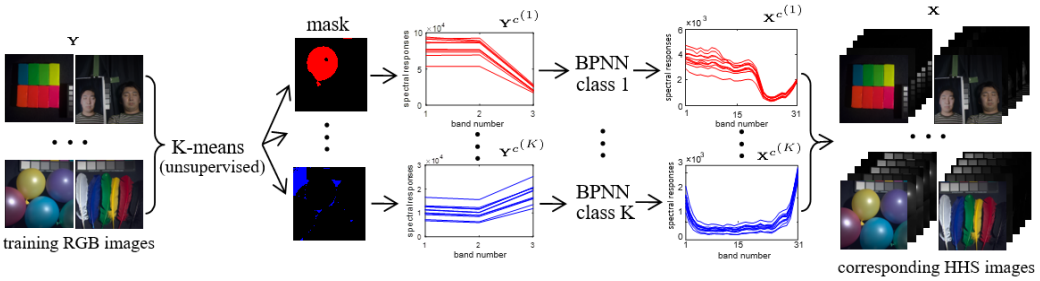

Fig.3 The training stage of our proposed method.

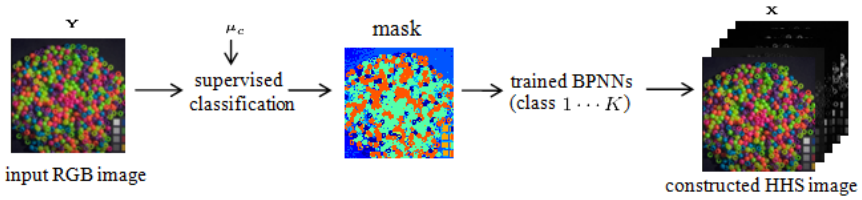

Fig.4 The spectral super-resolution stage of our proposed method.

Eq.(2), for each class, if the spectral mapping of spectrum-pairs from RGB to HHS can be learned by our proposed method, the spectrums of HHS image can be reconstructed from the corresponding ones of RGB image. The details of our proposed method are described as follows.

A. Associative Spectral classification for RGB image

The classification of RGB image $\mathbf{Y}$ can be described as the following minimization problem, using the minimum intra-class distance criterion:

$$\arg\min_{c,\boldsymbol{\mu}_c} \sum_{i=1}^{K} \sum_{\substack{j=1 \\ \boldsymbol{y}_j \in c^{(i)}}}^{N} d(\boldsymbol{y}_j, \boldsymbol{\mu}_{c^{(i)}}) \tag{3}$$

where $\boldsymbol{y}_j \in \mathbb{R}^3$ denotes the jth column (i.e., spectrum) of $\mathbf{Y}$, $\boldsymbol{\mu}_{c^{(i)}} \in \mathbb{R}^3$ denotes the clustering center of class i, and $d(\cdot)$ denotes the distance between the spectrums $\boldsymbol{y}_j$ and $\boldsymbol{\mu}_{c^{(i)}}$. In this paper, spectral correlation is employed as the measure of distance, defined as

$$d(\boldsymbol{y}_j, \boldsymbol{\mu}_{c^{(i)}}) = 1 - \cos\left(\frac{< \boldsymbol{y}_j, \boldsymbol{\mu}_{c^{(i)}} >}{||\boldsymbol{y}_j||_2 ||\boldsymbol{\mu}_{c^{(i)}}||_2}\right). \tag{4}$$

In the training stage, given the number of classes K, the above spectral classification problem in an RGB image can be viewed as an unsupervised clustering problem which can be solved by the k-means clustering algorithm [22].

In the spectral super-resolution stage, using the clustering center $\boldsymbol{\mu}_{c^{(i)}}$ determined during the training stage, each spectrum $\boldsymbol{y}_j$ of the input RGB image $\mathbf{Y}$ can be classified into the K clusters, by the following optimization problem:

$$\arg\min_{c} \sum_{i=1}^{K} d(\boldsymbol{y}_j, \boldsymbol{\mu}_{c^{(i)}}). \tag{5}$$

The above unsupervised clustering and supervised classification in the training and spectral super-resolution stage respectively, can be seen as an associative classification method carried out before the spectral mapping.

B. Class-based BP Neural Networks and Spectral Mapping

The spectral mapping from the classified RGB image to the corresponding HHS image in Eq.(2) is a challenging underdetermined inverse problem. To solve this problem, we treat it as a nonlinear spectral mapping to be represented by a BP neural network, which has a strong nonlinear mapping capability with a few hidden layers. A basic three-layer BP neural network used in this paper, including one hidden layer, is shown in Fig.2. The output of the BP neural network is

$$\boldsymbol{a_2} = l\big(\boldsymbol{w_2} g(\boldsymbol{w_1 a_0} + \boldsymbol{b_1}) + \boldsymbol{b_2}\big), \tag{6}$$

where $\boldsymbol{a_0}$ and $\boldsymbol{a_2}$ denote the inputs and outputs of BPNN respectively, $g(\cdot)$ denotes the nonlinear active function in the hidden layer, $l(\cdot)$ denotes the linear active function in the output layer, and $(\boldsymbol{w_1}, \boldsymbol{w_2}, \boldsymbol{b_1}, \boldsymbol{b_2})$ are the weights and offsets respectively.

We can see from the above that our proposed method first learns the nonlinear spectral mappings of spectrum-pairs of RGB and HHS images, and then can reconstruct the HHS image from only an RGB image. The two stages of overall framework of our proposed method are shown in Fig.3 and Fig.4, respectively. In the training stage shown in Fig.3, an unsupervised clustering is performed on the spectrums of RGB images. Then the classified spectrums of an RGB image and those of its corresponding HHS image form the spectrum-pairs for training different BPNNs for different classes, thereby establishing a nonlinear spectral mapping between RGB and HHS for each class. In the spectral super-resolution stage shown in Fig.4, after an associative spectral classification on the given RGB image, each spectrum in its corresponding HHS image is reconstructed by using the

established nonlinear spectral mapping of this corresponding class.

III. Experimental Results and Discussions

To evaluate the super-resolution performance of our proposed method, the relative state-of-the-art methods from Nguyen *et al.* [13], Galliani *et al.* [14], Arad *et al.* [8], Aeschbacher *et al.* [11] and Can *et al.* [15] are used for comparison on the ICVL [8], CAVE [24] and NUS [13] datasets. Additionally, seven full-reference quality metrics are used to evaluate the performance of each method, including spectral angle mapper (SAM) [20]; absolute RMSE, $RMSE_G$ and $RMSE_G^{uint}$; relative rRMSE, $rRMSE_G$ and $rRMSE_G^{uint}$ defined in [8], [14] and [15].

A. Datasets

The CAVE database [24] captured by a cooled CCD camera (Apogee Alta U260) has 32 images with a dimension of 512×512×31, ranging from 400 to 700 nm with 10 nm increments. Following the experiments of Galliani *et al.* [14], Aeschbacher *et al.* [11] and Can *et al.* [15], we use the CIE 1964 spectral response functions to simulate corresponding RGB images of the hyperspectral images.

The ICVL dataset [8] captured by a line scanner camera (Specim PS Kappa DX4 hyperspectral) includes 201 hyperspectral images with a dimension of 1392×1300 over 519 spectral bands (400-1000nm). To facilitate comparison and reduce computational costs [8], they are downsampled in the spectral domain with 31 bands from 400nm to 700nm with 10nm increments. We also use the CIE 1964 spectral response functions to simulate corresponding RGB images of the hyperspectral images, like in the original paper.

The NUS dataset [13] captured by a Specims PFDCL-65-V10E spectral camera contains 66 spectral images, ranging from 400 to 700nm, with 10nm increments. Following the experiments of Galliani *et al.* [14] and Aeschbacher *et al.* [11], Canon 1D Mark III spectral response functions are used to obtain the RGB images from the corresponding hyperspectral images.

B. Experimental Results

Since our proposed method learns the spectral mapping based on the classified spectrum-pairs, a different selection of training and test spectrums is used in this experiment. For the CAVE and ICVL datasets, instead of dividing the images into two sets [11], we divide the classified spectrums into two sets as 2-fold cross-validation. Similarly, for the NUS dataset, the classified spectrums are divided into a training set and a test set with the training/test split radio provided in [13]. In the training set, the spectrum-pairs are selected randomly from each class to training different BPNNs. For the fairness of the comparisons, the numbers of training and test spectrums used in our proposed method are the same with those of the method proposed by Aeschbacher *et al.* [11]. Additionally, in the training process, 85% of the training spectrum-pairs are used to train the BPNNs, and 15% of them are used as the validation data, to mitigate overfitting. Besides, the loss function in the training process is the mean squared error between the target spectrums and the mapped spectrums; the sigmoid function is used as the active function in the hidden layer, and a linear function is used in the output layer; the maximum training epochs is set to 100. According to different datasets and different numbers of training data, Table 1 shows the number of classes and the number of nodes in each layer of BPNNs for the three different datasets.

Table 1 Parameters in our proposed method on different datasets.

Datasets	CAVE [24]	ICVL [8]	NUS [13]
Number of training data	10000×16	2000×100	400×41
Number of classes	160	100	10
Number of nodes in BPNNs	3-10-31	3-20-31	3-6-31

Table 2 shows the quantitative spectral super-resolution results on the CAVE, ICVL and NUS datasets, in which the results of other related methods are all taken from their original papers, the short lines indicate that there are no relevant information available from the original papers, and the best results are shown in bold. It can be seen that our proposed method (marked as "CBPNN") shows a better spectral super-resolution results in both spectral and spatial domain than the other related methods under most metrics. Specifically, for the CAVE dataset, our proposed method outperforms other methods in RMSE and SAM. Particularly, RMSE is reduced over 1.1 than that of the other related methods, which indicates an outperformance in spatial preservation. Moreover, our proposed method improves the performance of spectral reconstruction over 4.7 in SAM than the method of [14], which is much significant for the HHS image. However, our proposed method performs a bit worse in rRMSE than the method of [15]. To further analyze the above results, a detailed analysis of the imaging quality of the CAVE dataset is shown in Fig.5, as an example. Figs.5(a) and (b) show the original glass tiles image from the CAVE dataset in band 31 and errors of the reconstructed glass tiles image using our proposed method in averaged rRMSE and zoomed in detail respectively. The visual results show that the dark strip on the left edge of glass tiles image is the major area with higher rRMSE errors. Besides, spectrums of the typical pixels with and without the dark strip are also shown in Figs.5(c) and (d), respectively. We can see from Figs.5(c) and (d) that, although the dark strip on the left edge of the glass tiles image has not provide much useful spectral information, it does result in large spectral super-resolution errors in rRMSE. During the experiments, we find that the above phenomenon appears in most images of the CAVE dataset; here we just took the glass tiles image as an example. In this case, we make an additional experiment using our proposed method, by simply deleting the left dark strip area with a size of 512×4 for the CAVE dataset, shown as the results of "CBPNN-d" in Table 2. The spectral super-resolution results in Table 2 show that the performance of our proposed method has achieved a great improvement, especially in rRMSE, and gives the best performance in relative RMSE than the other related methods. As for the methods of [14][15] using image patches, due to the large size of image patches, i.e. 36×36 or 64×64, only a 4 pixels wide dark strip at the edge may have a very limited effect on the performances of their spectral super-resolution

Table 2 Quantitative comparison on the CAVE, ICVL and NUS datasets. The best results are in bold, and the second best are underlined for ICVL.

	CAVE dataset [24]						ICVL dataset [8]					NUS dataset [13]					
	Galliani [14]	Arad [11]	A+ [11]	Can [15]	CBPNN	CBPNN-d	Galliani [14]	Arad [11]	A+ [11]	Can [15]	CBPNN	Nguyen [13]	Galliani [14]	Arad [11]	A+ [11]	Can [15]	CBPNN
RMSE	-	5.61	2.74	2.613	**1.5025**	1.5080	-	1.70	1.04	0.6324	**0.5754**	12.44	-	4.44	2.92	2.83	**2.4315**
$RMSE_G$	-	20.13	6.70	5.80	**3.8982**	3.9919	-	3.24	1.96	**1.33**	1.5433	8.06	-	9.56	5.17	4.92	**4.4231**
$RMSE_G^{uint}$	4.76	-	-	3.5275	**2.0364**	2.0401	1.98	-	-	1.23	**0.8676**	8.06	5.27	-	-	3.66	**2.9642**
rRMSE	-	0.4998	0.4265	0.178	0.3341	**0.1059**	-	0.0507	0.0344	0.0166	**0.0151**	0.2145	-	0.1904	0.1420	0.1471	**0.1365**
$rRMSE_G$	-	0.7755	0.3034	0.239	0.1396	**0.1393**	-	0.0837	0.0584	**0.0399**	0.0410	0.3026	-	0.3633	0.2242	0.2168	**0.1661**
$rRMSE_G^{uint}$	0.2804	-	-	0.1482	0.0891	**0.0857**	0.0587	-	-	0.0350	**0.0195**	0.3026	0.234	-	-	0.1747	**0.0931**
SAM	12.10	-	-	-	7.3467	**7.0159**	2.04	-	-	-	**1.1686**	-	10.11	-	-	-	**9.2271**

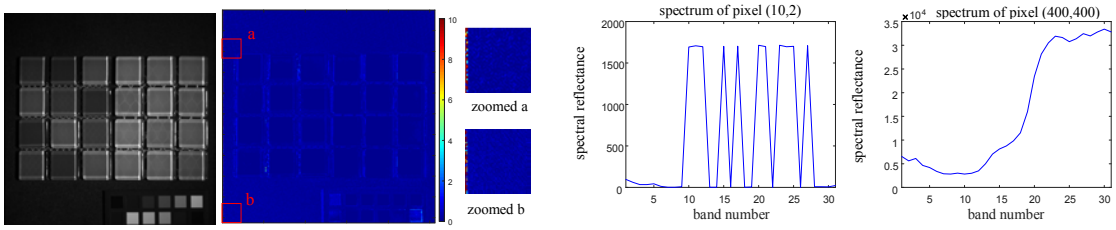

(a) (b) (c) (d)

Fig.5 Analysis results on a glass tiles image in the CAVE dataset: (a) original HHS image in band 31; (b) averaged rRMSE and zoomed in detail; spectrums of typical pixels (c) with and (d) without the dark strip on the left edge of (a).

Table 3 Training time and testing time for spectral super-resolution of one ICVL image with a size 1300×1392×31.

	Arad [8]	Arad [11]	A+ [11]	CBPNN
training time	-	2.8h	5.7h	**0.45h**
testing time	1.5h+100s	130s	110s	**15s**

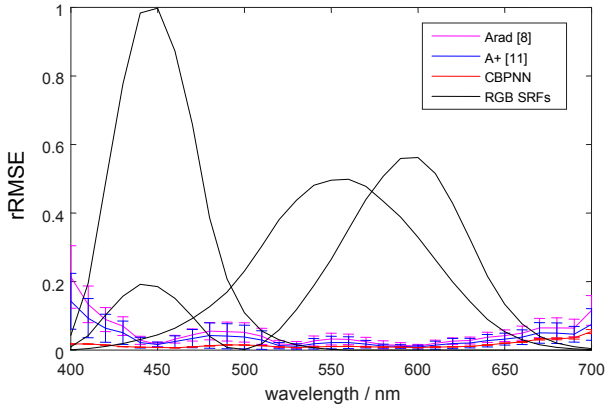

Fig.6 RGB SRFs and the averaged rRMSE at different wavelengths of three methods on the ICVL dataset.

results.

For the ICVL dataset, Table 2 also indicates the second best results (underlined). The spectral super-resolution results show that our proposed method is comparable to the method of [15] in $RMSE_G$ and $rRMSE_G$, and performs the best in terms of other quality metrics. Besides, to compare the spectral super-resolution results in rRMSE with the results provided by [8] and [11], Fig.6 shows the average and variance of rRMSE at different wavelengths, and the spectral response functions of the RGB image (RGB SRFs) are also provided. The results in Fig. 6 show that our proposed method performs best with the lowest rRMSE and the smallest variance compared with that of the methods [8] and [11], even in the wavelength ranges such as 400-420 nm, which are not well covered by the spectral response functions of the RGB image. Additionally, the training time and the testing time of different methods are shown in Table 3, which measure the time cost of the training step and the time required to reconstruct one image of the ICVL dataset. Our proposed method is conducted using MATLAB R2015b on a computer with a 3.60 GHz CPU and 28 GB RAM. Similarly to the method of [11], any vast parallelism has not been used in this comparison. The results in Table 3 indicate that, our proposed method uses much less training and testing time than the methods of [8] and [11]. Considering the better or comparable spectral super-resolution performances shown in Table 2, our proposed methods is more efficient with less computing time and better performances than the other related methods. Besides, for the NUS dataset, our proposed method performs the best in both spectral and spatial domains than all the other related methods. Particularly, SAM is reduced over 0.88 than the method of [14], and RMSE is reduced over 0.4 than all the other related methods. From the spectral super-resolution results in Table 2, we can see that our proposed method performs comparable or better than the recent shallow CNN approach of [15], and significantly better than the recent deep CNN and sparse representation method of [11] and [8], and the approach of [13]. Additionally, the spectral super-resolution performance of our proposed method on typical spectrums of different datasets is shown in Fig.7. As can be seen in Fig.7, the spectrums are reconstructed with high accuracy using our proposed method.

C. Discussion on Parameters Selection

To evaluate the effect of the number of classes K on the spectral super-resolution performance of our proposed method, the averaged RMSE and SAM curves of the reconstructed spectrums of HHS images on the CAVE dataset are shown in

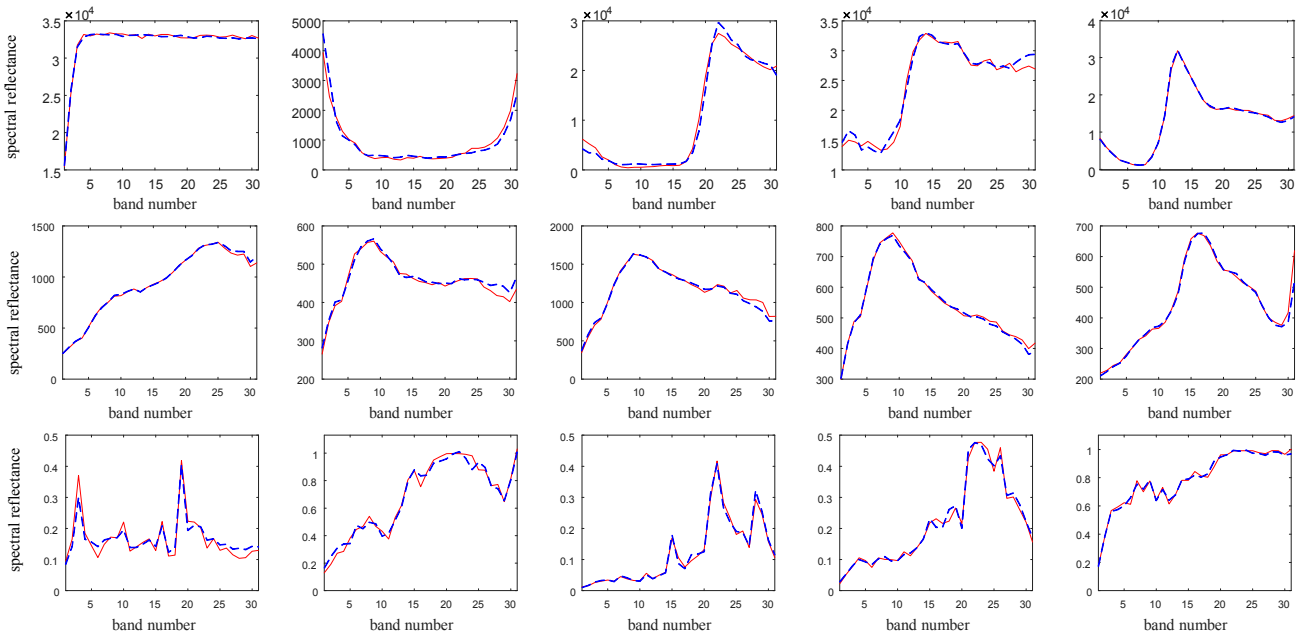

Fig.7 Spectrums of the ground truth (red) and the reconstructed result by our proposed method (blue, dashed) on typical pixels of the CAVE (the first row), ICVL (the second row) and NUS (the third row) datasets.

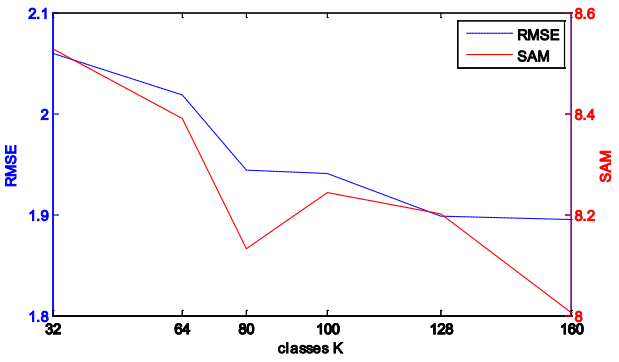

Fig.8 RMSE and SAM curves on the CAVE dataset as a function of K.

Fig.8, as a function of K. As shown in Fig.8, with the increase of K, the RMSE and SAM curves show a downward trend to some extent. It indicates that the reconstructed spectrums of our proposed method can preserve more spatial and spectral information when the number of classes increases. This may be due to the fact that, with more classes, the similarity of spectrums in each class is increased, which is more conducive for BPNNs to learn the spectral mapping in each class, and will further improve the quality of the reconstructed spectrums.

IV. Conclutions

In this paper, we proposed a new spectral super-resolution method to reconstruct an HHS image from an RGB image using class-based BPNNs. In this method, BPNNs are used to learn nonlinear spectral mappings using the classified spectrum-pairs of RGB images and their corresponding HHS images. Then for a given test RGB image, each spectrum in its HHS counterpart is reconstructed from the classified given RGB image using the trained BPNNs. Besides, an associative spectral classification is adopted to ensure the consistency of classes in the training stage and the spectral super-resolution stage. Experimental results on three standard datasets demonstrate that our proposed method achieves a better spectral super-resolution quality than that of the other state-of-the-art methods.

References

[1] L. Qin, X. Wang, J. Jiang, X. Yang, D. Ke, H. Li, and D. Wang, "Use hyper-spectral remote sensing technique to monitoring pine wood nomatode disease preliminary," *International Symposium on Optoelectronic Technology and Application 2016*. International Society for Optics and Photonics, 2016.

[2] T. Arnold, R. Leitner, and G. Bodner, "Application of NIR hyperspectral imaging for water distribution measurements in plant roots and soil," *In SENSORS, 2016 IEEE*, pp. 1-3, October, 2016.

[3] M. Jiang, F. Cao, and Y. Lu, "Extreme Learning Machine with Enhanced Composite Feature for Spectral-Spatial Hyperspectral Image Classification," *IEEE Access*, vol. 6, pp. 22645-22654, 2018.

[4] A. Qin, Z. Shang, J. Tian, T. Zhang, Y. Y. Tang, and J. Qian, "Edge-Smoothing-Based Distribution Preserving Hyperspherical Embedding for Hyperspectral Image Classification," *IEEE Journal of Selected Topics in Applied Earth Observations and Remote Sensing*, 2018.

[5] M. Díaz, R. Guerra, S. López, and R. Sarmiento, "An Algorithm for an Accurate Detection of Anomalies in Hyperspectral Images With a Low Computational Complexity," *IEEE Transactions on Geoscience and Remote Sensing*, vol. 56, no. 2, pp. 1159-1176, 2018.

[6] S. Matteoli, M. Diani, and G. Corsini, "Automatic Target Recognition Within Anomalous Regions of Interest in Hyperspectral Images," *IEEE Journal of Selected Topics in Applied Earth Observations and Remote Sensing*, vol. 11, no. 4, pp. 1056-1069, 2018.

[7] N. Akhtar, F. Shafait, and A. Mian, "Sparse spatio-spectral representation for hyperspectral image super-resolution," *IEEE ECCV*, pp. 63-78, 2014.

[8] B. Arad and O. Ben-Shahar, "Sparse recovery of hyperspectral signal from natural RGB images," *In European Conference on Computer Vision,* pp. 19–34. Springer, 2016.

[9] M. Aharon, M.Elad, and A. Bruckstein, "K-SVD: An Algorithm for Designing Overcomplete Dictionaries for Sparse Representation," *IEEE Transactions on signal processing*, vol. 54, no. 11, pp. 4311-4322, 2006.

[10] R. Rubinstein, M. Zibulevsky, and M. Elad, "Efficient implementation of the K-SVD algorithm using batch orthogonal matching pursuit," *Cs Technion,* vol. 40, no. 8, pp. 1-15, 2008.

[11] J. Aeschbacher, J. Wu, and R. Timofte, "In defense of shallow learned spectral reconstruction from rgb images," in *ICCV Workshops*, Oct 2017.

[12] R. Timofte, V. De Smet, and L. Van Gool, "A+: adjusted anchored neighborhood regression for fast super-resolution," in *ACCV*, pp. 111–126, 2014.

[13] R. M. Nguyen, D. K. Prasad, and M. S. Brown. "Training-based spectral reconstruction from a single rgb image," *In European Conference on Computer Vision*, pp. 186–201. Springer, 2014.

[14] S. Galliani, C. Lanaras, D. Marmanis, E. Baltsavias, and K. Schindler, "Learned spectral super-resolution," arXiv preprint arXiv: 1703.09470, 2017.

[15] Y. B. Can and R. Timofte, "An efficient CNN for spectral reconstruction from RGB images," arXiv preprint arXiv: 1804.04647, 2018.

[16] R. Timofte, R. Rothe, and L. Van Gool, "Seven ways to improve example-based single image super resolution," in *CVPR*, June 2016.

[17] R. Hecht-Nielsen, "Theory of the backpropagation neural network," In *Neural networks for perception*, vol. 1, pp. 593-605, 1989.

[18] F. A. Mianji, Y. Zhang, and A. Babakhani, "Superresolution of hyperspectral images using backpropagation neural networks," *In Nonlinear Dynamics and Synchronization, INDS'09, 2nd International Workshop on.* IEEE. pp. 168-174, July, 2009.

[19] L. Xiu, H. Zhang, Q. Guo, Z. Wang, and X. Liu, "Estimating nitrogen content of corn based on wavelet energy coefficient and BP neural network," *In Information Science and Control Engineering (ICISCE), 2015 2nd International Conference on.* IEEE. pp. 212-216, April, 2015.

[20] Q. Wei, J. Bioucas-Dias, N. Dobigeon, and J.Y. Tourneret, "Hyperspectral and Multispectral Image Fusion Based on a Sparse Representation," *IEEE Transactions on Geoscience and Remote Sensing*, vol. 53, no. 7, pp. 3658–3668, Jul. 2015.

[21] F. Palsson, J. R. Sveinsson, and M. O. Ulfarsson, "Multispectral and hyperspectral image fusion using a 3-D-convolutional neural network," *IEEE Geoscience and Remote Sensing Letters*, vol. 14, no. 5, pp. 639-643, 2017.

[22] H. Spath, *The cluster dissection and analysis theory fortran programs examples*. Prentice-Hall, Inc., 1985.

[23] Z. Wang, A. C. Bovik, H. R. Sheikh, and E. P. Simoncelli, "Image quality assessment: from error visibility to structural similarity." *IEEE transactions on image processing,* vol. 13, no. 4, pp. 600-612, 2004.

[24] F. Yasuma, T. Mitsunaga, D. Iso, and S. K. Nayar. "Generalized assorted pixel camera," Technical report, Tech. Report, Department of Computer Science, Columbia University, 2008.